Mapping tropospheric ozone profiles from an airborne ultraviolet–visible spectrometer

Xiong Liu, Christopher E. Sioris, Kelly Chance, Thomas P. Kurosu, Michael J. Newchurch, Randall V. Martin, and Paul I. Palmer

We present a novel technique for retrieving ozone (O_3) profiles and especially tropospheric O_3 from airborne UV/visible spectrometer measurements. This technique utilizes radiance spectra from one down-looking and two up-looking (85° and 75°) directions, taking advantage of the O_3 absorption structure in the Huggins (300–340-nm) and Chappuis (530–650-nm) bands. This technique is especially sensitive to tropospheric O_3 below and ≤8 km above the aircraft with a vertical resolution of 2–6 km and is sensitive to lower and middle stratospheric O_3 with a vertical resolution of 8–15 km. It can measure tropospheric O_3 at spatial resolutions of 2 km × 2 km or higher and is therefore well suited for regional air-quality studies and validation of satellite measurements.   © 2005 Optical Society of America

OCIS codes: 010.4950, 010.7030, 280.1120, 000.2170.

1. Introduction

Ozone plays a key role in the chemical processes and energy budget of the troposphere.[1,2] Because of the sparse distribution of *in situ* observations and the large spatial and temporal variability of tropospheric ozone (O_3), remote-sensing techniques are crucial for studying its distributions, photochemical sources and sinks, transport, and seasonal behavior.

Current remote-sensing instruments typically provide a total column O_3 abundance. Retrieving the tropospheric column O_3 requires estimating and subtracting the upper portion of the total column. Most current tropospheric O_3 retrievals use this residual-based method,[3–16] but they are subject to significant uncertainties in the assumptions made in estimating the upper portion of column O_3 and to relatively coarse spatial resolution (>1° longitude × 1° latitude) and temporal resolution (i.e., monthly). These different techniques can differ significantly from one another by as much as 20 Dobson Units (DU) (1 DU = 2.687 × 10^{16} molecules cm^{-2}) in some critical areas (e.g., North Africa near the tropics, a region of intense biomass burning during December–February) and also disagree in important respects with the current model calculations of the tropospheric O_3.[17] Direct retrieval of tropospheric O_3 from space has been demonstrated with Global Ozone Monitoring Experiment (GOME) spectra but with coarse vertical (10–15 km) and spatial (960 km × 80 km or 320 km × 40 km) resolution.[18–22]

Because satellite-based measurements of tropospheric O_3 usually have a spatial resolution coarser than tens of kilometers (e.g., the highest resolution for tropospheric O_3 is currently from an Ozone Monitoring Instrument (OMI) with a resolution of 13 km × 24 km at nadir), intermediate-scale measurements (between *in situ* measurements and satellite observations) are lacking. However, the lifetimes of tropospheric O_3 and many of its reactive precursors are long enough that atmospheric transport plays an important role in their atmospheric distribution. It is therefore difficult to relate the *in situ* observations to larger spatial scales and to validate area satellite measurements against point *in situ* measurements. Spectroscopic remote sensing from aircraft offers a unique capability to measure gases on intermediate spatial scales, thereby filling the gap between *in situ* measurements and space-borne observations.

Since the late 1980s airborne remote sensing has

X. Liu, C. E. Sioris, K. Chance, T. P. Kurosu, and R. V. Martin are with the Atomic and Molecular Physics Division, Harvard-Smithsonian Center for Astrophysics, Cambridge, Massachusetts 02138 (e-mail for X. Liu, xliu@cfa.harvard.edu). M. J. Newchurch is with the Department of Atmospheric Science, University of Alabama in Huntsville, Huntsville, Alabama 35805. P. I. Palmer is with the Division of Engineering and Applied Sciences, Harvard University, Cambridge, Massachusetts 02138. R. V. Martin is also with the Department of Physics and Atmospheric Sciences, Dalhousie University, Halifax, Nova Scotia B3H 3J5, Canada.

been used to measure the column abundances of trace gases (e.g., O_3, NO_2, $OClO$, BrO) from UV/visible zenith-sky absorption spectra with the differential optical absorption spectroscopy (DOAS) approach.[23–28] Jiang et al.[29] demonstrated the concept of retrieving tropospheric O_3 by using ratios of diffuse radiances (i.e., both zenith and off-axis angle radiances) to direct irradiances from ground-based measurements. The larger multiple-scattering effects in the troposphere compared with those in the stratosphere greatly enhance the optical path length of tropospheric O_3, thus making the ratios of diffuse radiances to direct irradiances sensitive to tropospheric O_3 and insensitive to stratospheric O_3. Recently off-axis measurements with an airborne UV/visible spectrometer have been taken to retrieve trace-gas concentrations. Petritoli et al.[30] measured O_3 concentrations near the flight altitude from measured UV spectra at three angles (one near zenith and two near horizontal) in which the zenith-sky spectrum was used as a reference. The Airborne Multiaxis Differential Optical Absorption Spectroscopy (AMAXDOAS) instrument is configured to take UV/visible measurements from as many as 10 viewing zenith angles (0°, 60°, 80°, 85°, and 88° for both up-looking and down-looking directions).[31] This instrument can separate the tropospheric and stratospheric portions of a significant number of gases (O_3, NO_2, $OClO$, BrO, SO_2, $HCHO$).[31] Bruns et al.[32] performed sensitivity studies to show that profile information for NO_2 can be obtained from this instrument. The NO_2 slant column densities are first fitted by using the DOAS approach at these 10 angles with an external solar reference spectrum; then a vertical profile is derived by using the optimal estimation approach by matching the calculated and derived slant-column densities.

In this paper we introduce a novel method for accurately retrieving tropospheric O_3 profiles from airborne UV/visible spectrometer measurements with the optimal estimation approach.[33] This tropospheric retrieval utilizes O_3 absorption in the Huggins (300–340-nm) and Chappuis (530–650-nm) bands from measurements at three viewing zenith angles (VZAs): any down-looking angle that intercepts the surface and two up-looking directions at VZAs of 85° and 75°. Radiance spectra are normalized to direct irradiances or zenith-sky radiances so that no external solar reference spectra are needed. Ozone profiles can be resolved with moderate vertical resolution (2–6 km) in the troposphere and vertical resolution of 8–15 km in the lower and middle stratospheres. Because only one down-looking angle is needed, the airborne spectrometer can be designed to scan spatially, as some satellite instruments such as GOME and the Scanning Imaging Absorption Spectrometer for Atmospheric Chartography (SCIAMACHY) do. With the scanning capability of the proposed airborne instrumentation, tropospheric O_3 profiles can be mapped with spatial resolutions of 2 km $\times$ 2 km at nadir or even higher.

2. Instrument Design and Configuration

This technique is based on a proposed instrument, the Tropospheric Optical Spectrometer (TROPSPEC). TROPSPEC is a UV/visible array detector-based spectrometer system, consisting of four spectrographs measuring above and below the aircraft with a 0.2-nm FWHM spectral resolution from 300 to 400 nm (the UV channel) and a 0.6-nm resolution from 400 to 700 nm (the visible channel). The spectral sampling is assumed to be 0.05 and 0.15 nm/pixel for these regions, respectively. TROPSPEC scans about the aircraft roll axis: The down-looking UV and visible spectrographs measure across the flight track, and the up-looking UV and visible spectrographs measure at different zenith angles. For the results presented below the integration time is 10 s and the instantaneous field of view is 7.6°. The direct irradiance at flight altitude is also measured with a diffuser plate by applying the rotating shadow-band technique.[34] This configuration gives a spatial resolution of 2 km $\times$ 2 km at nadir for down-looking measurements, assuming a flight altitude of 15 km and a flight speed of 700 km/h. If the instrument scans to an off-axis angle of 79.8°, the swath across the flight direction is $\sim$166.0 km. This high spatial resolution and superior spatial coverage make TROPSPEC well suited for satellite validation and regional air-quality monitoring. The estimated measurement errors are based on current detector technology and radiances modeled with GOME and SCIAMACHY heritage as guidance. The signal-to-noise ratios (S/N) of both up-looking and down-looking measurements at 300, 340, and 600 nm are $\sim$250, 3000, and 2000, respectively, for the above flight configuration, assuming the U.S. standard atmosphere with LOWTRAN background aerosols[35] (aerosol optical thickness is $\sim$0.14 at 550 nm with background stratospheric aerosols and a visibility of 50 km in the troposphere), a surface albedo of 0.10, and a solar zenith angle (SZA) of 45°. In addition to the O_3 profile retrieval presented below, stratospheric and tropospheric columns of several trace gases can be measured, like AMAXDOAS but with a larger across-track swath. Aerosol properties can be retrieved with Total Ozone Mapping Spectrometer (TOMS)-like[36] and Moderate Resolution Imaging Spectroradiometer (MODIS)-like approaches[37] from the UV and the visible spectra, respectively, and cloud information can also be obtained from spectra inside and outside absorption features of the O_2–O_2 collision complex.[38] The aerosol and cloud information can be further used to correct gas trace-gas retrieval.[39]

3. Methodology for Ozone Profile Retrieval

In the remote sensing of O_3 and other species, typically a reference spectrum is necessary to normalize the measured radiance spectra (i.e., taking the ratio of the radiance spectra to the reference spectrum before retrieval or synthesizing the radiance spectrum beginning with the reference spectrum). For our method either the direct irradiance or the zenith-sky radiance can serve this purpose. This normalization

not only serves as relative radiometric and wavelength calibrations but also reduces interference from stratospheric aerosols on retrieval because the effect is common to both reference and target spectra. When a zenith-sky reference is used the normalization minimizes the Ring effect for a similar reason. We use the wavelength and the temperature-dependent O_3 absorption structure in the Huggins bands[40] (i.e., 300–340 nm) and the weak O_3-absorbing Chappuis bands (i.e., 530–650 nm) for O_3 profile retrieval.

To describe the physical principles of our technique, we introduce the commonly used concept of the air mass factor (AMF), which is defined here as the ratio of the average path length for photons intercepted by the spectrometer in a particular atmospheric layer to the vertical thickness of the layer. The AMF at a certain layer i can be linked to the radiance change ($\Delta I = I' - I$) after the O_3 absorption optical thickness is perturbed by a small amount $\Delta\tau_i$ at that layer:

$$\frac{I'}{I} \approx \exp(-\mathrm{AMF}_i \times \Delta\tau_i). \quad (1)$$

The AMF for that layer can be approximated as

$$\mathrm{AMF}_i \approx -\frac{\ln I' - \ln I}{\Delta\tau_i} \approx -\frac{\Delta I}{I\Delta\tau_i} \approx -\frac{dI}{Id\tau_i} = -\frac{dI}{I\beta_i dx_i}, \quad (2)$$

where β_i is the absorption optical thickness per DU of O_3, x_i is the column O_3 in that layer, and dI/dx_i gives the weighting function of the radiance with respect to ozone in the ith layer. For the direct irradiance reference the AMF is just the geometric AMF above the aircraft and zero below the aircraft; for the zenith-sky radiance reference the AMF can be similarly calculated according to Eq. (2). Then the AMF for a normalized radiance is the AMF difference between the unnormalized radiance and the reference.

We use the linearized discrete ordinate radiative transfer[41] (LIDORT) model to calculate radiances, weighting functions, and therefore AMFs. It is also used as the forward model to simulate radiances and weighting functions during the retrieval process. In the version of LIDORT used here the pseudo-spherical approximation is applied, and the effect of polarization on radiances is not considered.

Figure 1 shows the AMFs for down-looking radiances (VZA, 0°) and up-looking radiances (VZA, 75°, 85°) normalized by both direct irradiances [Figs. 1(a), 1(c), 1(e)] and zenith-sky radiances [Figs. 1(b), 1(d), 1(f)] at selected wavelengths for a flight altitude of 15 km. For down-looking radiances [Figs. 1(a) and 1(b)] we can see that the AMFs above the aircraft are almost zero; thus the normalization removes most of the information above the aircraft, leaving the information below the aircraft. With the decrease in O_3 absorption in the Huggins bands at longer wave-
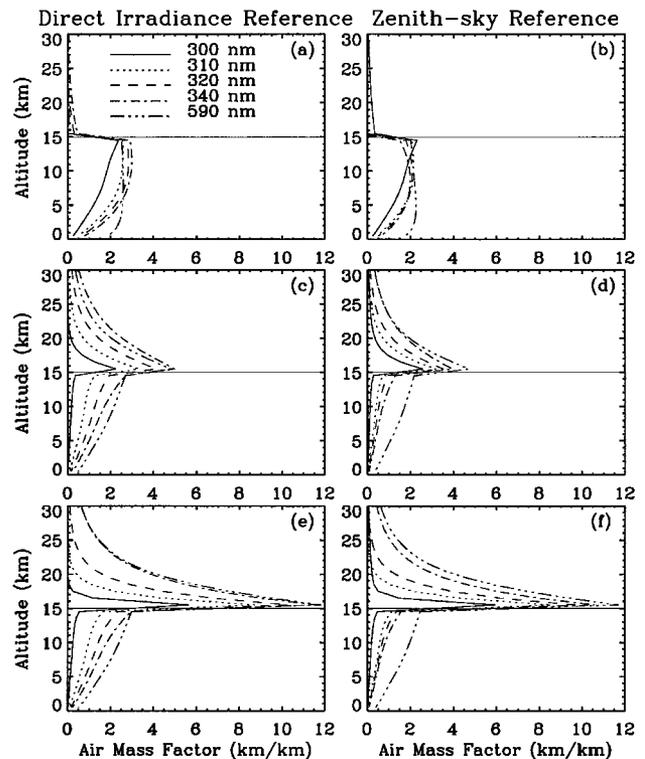

Fig. 1. (a) Air mass factors (kilometer/kilometer) for down-looking radiances with a VZA of 0° at 300, 310, 320, 340, and 590 nm normalized to the direct irradiance reference. (b) Similar to (a) but for radiances normalized to zenith-sky radiance reference. (c)–(d), (e)–(f) Similar to (a)–(b) but for up-looking radiances at a VZA of 75° and 85°, respectively. Calculation is performed for the U.S. Standard Atmosphere with a total O_3 of 345.3 DU and LOWTRAN background aerosols. The SZA is 45°, and the surface albedo is 0.1. Flight altitude is 15.0 km. The AMF is calculated on an altitude grid from 0 to 60 km at every 1 km.

lengths, measured backscattered photons penetrate deeper into the surface (i.e., increasing AMF near the surface). In the Chappuis bands (e.g., 590 nm) AMFs are almost altitude-independent below the aircraft, indicating that normalized down-looking radiances are sensitive to the total column O_3 below the aircraft. Because of wavelength-dependent penetration, together with the temperature-dependent O_3 absorption structure in the Huggins bands[40] and the weak O_3-absorbing structure in the Chappuis bands, tropospheric O_3 profiles below the aircraft can be resolved and column O_3 down to the surface can be measured.

For up-looking radiances [Figs. 1(c)–1(f)] the normalization cancels most of the information at certain altitudes (called canceling altitudes) above the aircraft. Photons measured by the spectrometer have experienced mainly single scattering above those altitudes for different VZAs (including zenith) and therefore have optical path lengths close to those for direct irradiances. Below the canceling altitudes the AMFs increase with decreasing altitudes down to the flight altitude because of enhanced multiple scattering in up-looking radiances

with relation to zenith-sky radiances or direct irradiances. The location of the canceling altitude and the magnitude of the normalized AMF are determined by the competition between scattering into the line of sight and extinction (i.e., absorption and scattering out of the line of sight). Because of the strong variation in O_3 absorption and Rayleigh scattering with wavelength, the altitude range of canceling and the degree of cancellation are especially wavelength dependent in the Huggins bands. Therefore, because of the wavelength-dependent O_3 absorption features, the normalized up-looking radiance spectrum contains valuable profile information above the aircraft.

In addition the location of canceling altitudes and the residual sensitivity to information above also depend on the VZA because larger path lengths for larger VZAs further enhance the above competing processes. As we see from Figs. 1(c)–1(f) a larger VZA provides greater sensitivity to information above mainly because of the larger path length along the line of sight. To extract valuable information above the aircraft, radiances measured at large off-axis angles have to be utilized to provide more sensitivity to overhead O_3; thus up-looking angles of 85° and 75° are selected. An up-looking angle of 75° provides more sensitivity to O_3 at higher altitudes compared with an up-looking angle of 85°; for example, the AMFs at ~25 km are larger for 75° than for 85° at those UV wavelengths. We find that using additional measurements from other off-axis angles improves the retrieval only minimally.

Note that the AMFs for normalized up-looking radiances at 75° and 85° are still significant, suggesting that the normalized radiances still have significant sensitivity to information below the aircraft due to multiple scattering from below the aircraft; this cannot be canceled by normalization because the direct irradiance (zenith-sky radiance) experiences no (less) multiple scattering.

The direct irradiance is insensitive to information below the aircraft while the zenith-sky radiance is still sensitive to O_3 below the aircraft because of multiple-scattering effects, so that using the direct irradiance as a reference gives more sensitivity to information below the aircraft than using the zenith-sky reference. However, this sensitivity below the aircraft leads to interference when up-looking radiances are used to retrieve ozone information above the aircraft. Above the aircraft the AMF for zenith-sky radiance may be smaller or larger than the geometric AMF depending on wavelength and viewing geometry; thus using a zenith-sky reference may provide more or less O_3 sensitivity than using the direct irradiance reference.

O_3 profile retrieval is an ill-conditioned problem; i.e., there are no unique solutions for the measurements. We use Rodgers' optimal estimation[33] for the inversion of normalized radiance spectra at three angles to obtain the best solution. Some basics of the optimal estimation are reviewed as follows, and the reader is referred to Rodgers[33] for more detail. The
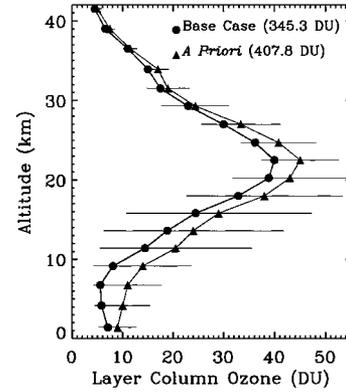

Fig. 2. O_3 profile for the standard case and *a priori* O_3 profile used in the retrievals. *A priori* standard deviations [i.e., $S_a(i, i)^{1/2}$ in Eq. (4)] in the equations are plotted as error bars. The total column O_3 is shown in parentheses.

solution for the nonlinear problem is

$$X_{k+1} = X_k + (K^T S_\varepsilon^{-1} K + S_a^{-1})^{-1}\{K^T S_\varepsilon^{-1}[Y - F(X_k)] - S_a^{-1}(X_k - X_a)\}, \quad (3)$$

where X_{k+1} and X_k are the current and the previous state vectors, respectively; K is the weighting function matrix; S_ε is the measurement error matrix (often assumed diagonal, i.e., no correlation in the measured errors between adjacent wavelengths); X_a is the *a priori* state vector; and S_a is the *a priori* covariance matrix. X_a and the diagonal of S_a (i.e., O_3 variance) can be derived from O_3 climatology, and the off-diagonal elements of S_a can be constructed by using the height correlation:

$$S_a(i, j) = [S_a(i, i)S_a(j, j)]^{1/2} \exp(- |z_i - z_j| / l), \quad (4)$$

where z_i are z_j are the altitudes for layer i and j and l is the correlation length. The averaging kernel matrix (A) is defined as the sensitivity of the retrieved state X' to true state X, a useful concept for characterizing the retrieval:

$$A = dX'/dX = (K^T S_\varepsilon^{-1} K + S_a^{-1})^{-1} K^T S_\varepsilon^{-1} K. \quad (5)$$

The trace of the averaging kernel matrix is called the degrees of freedom for signal (DFS), which describes the number of pieces of information available from the set of measurements. The diagonal elements of the averaging kernels indicate the DFS at each layer.

4. Results and Discussion

To present the capability of this technique for O_3 profile retrieval, the simulations and retrievals are done on the following standard case: a U.S. Standard Atmosphere with a total O_3 of 345.3 DU (Fig. 2), clear-sky, LOWTRAN background aerosols, a surface albedo of 0.1, a SZA of 45°, with the direct irradiance as a reference, and with the instrumental characteristics presented in Section 2. The atmosphere is mod-
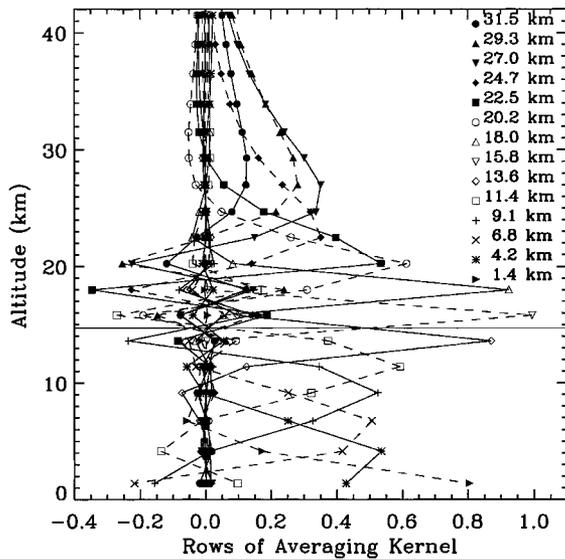
Fig. 3. Averaging kernels for the standard case. The horizontal line shows the flight altitude. The averaging kernels at different altitudes are plotted as solid and dashed lines alternately.

Table 1. Degrees of Freedom for Signal at Each Layer, Actual Peak Altitude of the Averaging Kernels, Vertical Resolution in Terms of FWHM for Each Row of Averaging Kernels of the Base Case

NA[a] (km)	DFS	PA[b] (km)	VR[c] (km)
1.4	0.80	1.4	3.5
4.2	0.54	4.2	5.3
6.8	0.51	6.8	5.2
9.1	0.53	9.1	6.1
11.4	0.59	11.4	5.4
13.6	0.87	13.6	2.9
15.8	0.99	15.8	2.3
18.0	0.92	18.0	2.5
20.3	0.61	20.3	4.7
22.5	0.40	20.3	5.5
24.7	0.32	22.5	8.0
27.0	0.35	24.7	9.5
29.3	0.27	27.0	12.6
31.5	0.11	29.3	14.5

[a]Nominal altitude, which is the middle altitude of a layer.
[b]Peak altitude.
[c]Vertical resolution.

eled, and the O_3 profile is retrieved on an Umkehr-type grid with 22 layers from 0 to ~60 km, ~2.5 km for each of the bottom 20 layers, and ~5 km for the top two layers. Because the retrieval grid is different from the very finely spaced atmospheric grid in the AMF calculation shown in Fig. 1, we use a flight altitude of 14.7 km (i.e., top of the sixth layer on the retrieval grid) for the standard case, approximately consistent with the flight altitude of 15.0 km in Fig. 1. We perform sensitivity studies for various different parameters by modifying the standard case.

For all simulations of measured radiances the estimated measurement noise is added before the inversions. Partial O_3 columns for the top four layers are not retrieved but are fixed to values used in the simulation, since there is almost no sensitivity to O_3 above this altitude, and in practice this information is readily available from satellite observations. The *a priori* O_3 profile is shown in Fig. 2. It is constructed so that it deviates from the standard profile more at altitude regions with strong O_3 sensitivity in our method and is closer to the standard O_3 profile at higher altitudes. The *a priori* standard deviations used in the retrievals are taken from the TOMS Version 8 climatology[42] at mid-latitude during winter and are also plotted in Fig. 2 as error bars. A correlation length of 5 km is used to construct the *a priori* covariance matrix according to Eq. (4). Because the focus of this study is to show the optimal performance of the O_3 profile retrieval, the Ring effect, undersampling, and other minor species (e.g., NO_2, SO_2, H_2O) are not considered in the simulations and retrievals, and the atmospheric conditions (e.g., pressure, temperature, aerosols) except the O_3 profile are assumed to be known.

Figure 3 shows the averaging kernels at altitudes as high as ~31.5 km for the base case. The averaging kernels for higher altitudes are not shown because the

available information is negligible and the DFS at those layers are < 0.1. Table 1 shows the DFS at each layer, the actual peak altitude of the averaging kernels, and the vertical resolutions in terms of FWHM, which are derived from the averaging kernels in Fig. 3. From the surface to ~23 km the vertical resolution is less than ~6 km; the peak altitudes of the averaging kernels usually agree with the actual nominal altitudes. The DFS at each of those layers is greater than 0.5. The retrieval is particularly sensitive to O_3 near the flight altitude with a retrieval sensitivity greater than 0.85 and with a vertical resolution in the range of 2–3 km. Below the flight altitude the retrieval sensitivity first decreases with decreasing altitude, then increases toward the surface because of increasing photo path enhancement from interaction between surface reflection and atmospheric scattering in the lowest atmospheric layers. Above the flight altitude the vertical resolution becomes greater with increasing altitude, and the peak altitude shifts to a lower altitude because of reduced O_3 sensitivity. For example, the vertical resolution increases from 5.5 km at 23 km to ~14.5 km at ~32 km.

Figure 4(a) shows the retrieved O_3 profiles for the base case together with the true and *a priori* O_3 profiles, and Fig. 4(b) shows the column O_3 bias in retrieval. Figures 4(c)–4(d) and 4(e)–4(f) show similar comparisons but for two modified cases with low and high amounts of tropospheric O_3, respectively. The low tropospheric O_3 case has 19.0 DU of O_3 below the aircraft and an average O_3 mixing ratio of ~10 parts per billion by volume (ppbv) in the near-surface layer; the high tropospheric O_3 case has 109.0 DU of O_3 below the aircraft and an average O_3 mixing ratio of ~125 ppbv on the near-surface layer. The retrieved profiles agree well with the true profiles for all cases. The alternating deviations of the retrievals for the two modified profiles are present mainly because the
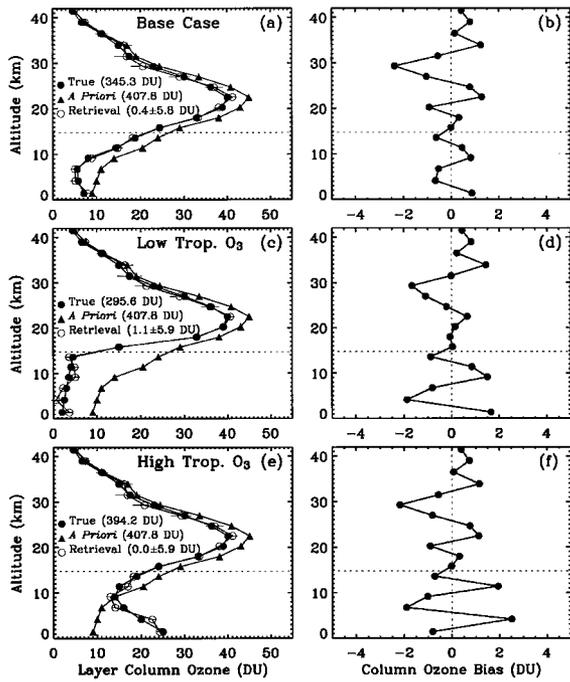
Fig. 4. (a) True, *a priori*, and retrieved O_3 profiles for the base case. (b) Column O_3 bias between retrieved and true profiles in (a). (c)–(d), (e)–(f) Similar to (a)–(b) but for two modified cases with low and high tropospheric O_3 conditions, respectively. The total O_3 for the true and *a priori* O_3 profiles and the total O_3 bias in the retrieval are shown in parentheses. The error bars on retrievals include both random-noise errors and smoothing errors.

a priori profile shape is different from the true profile shapes and the information from the measurements is inadequate for resolving each individual layer. The biases in total O_3 and O_3 below the aircraft are less

than 1.0 and 0.5 DU, respectively, with the sum of random-noise retrieval and smoothing errors less than 6.0 and 0.3 DU for all three cases. In the lower troposphere the retrieved profiles for the two modified cases are outside the standard deviations of *a priori* values. These retrievals provide evidence of the strong sensitivity of this technique to O_3 in the troposphere and its insensitivity to *a priori* information.

We have investigated the sensitivities of this approach to viewing geometry, surface albedo, reference normalization, aircraft altitude, measurement error, and spectral resolution. Table 2 shows the retrieved biases (i.e., the difference between retrieved and true values) in total O_3, O_3 above and below the aircraft, and DFS for the whole profile and DFS for below the aircraft for different plans. The column entitled cases lists only the difference between each plan and the base case. An important advantage of this technique is that it does not require a high spectral resolution. Reducing the spectra resolution from 0.2- to 1.0-nm FWHM and reducing the spectral sampling from 0.1 to 0.4 nm/pixel decrease the DFS by only ~0.5 for the whole profile and by 0.2 for the profile below the aircraft. The fact that increasing the spectral resolution only slightly improves the retrievals suggests that the O_3 information from this technique mainly originates from broad O_3 absorption features instead of those fine structures in the Huggins bands. With the increase in measurement errors, the retrieval performance decreases as expected. For example, when the S/N is reduced by a factor of 5, the DFS is reduced by 1.5 for the whole profile and 0.8 for the profile below the aircraft and retrieval errors increase, but this technique can still accurately measure tropospheric O_3 profiles and the column below the aircraft. The performance is slightly worse when

Table 2. Column O_3 Biases with Retrieval Errors due to Measurement Random Noise and Smoothing

Cases[a]	Column O_3 Bias (DU)			
	Total	Below	Above	DFS
Base case	0.4 ± 5.9	0.3 ± 0.3	0.1 ± 4.3	7.4/3.5
1.0-nm FWHM, 0.4-nm/pixel	4.6 ± 6.6	−0.2 ± 0.3	4.8 ± 5.4	6.9/3.3
Zenith reference	0.8 ± 6.2	0.5 ± 0.5	0.3 ± 5.0	7.0/3.2
0.2 times S/N	1.2 ± 8.2	0.9 ± 1.0	0.3 ± 7.6	5.9/2.7
Solar reference	0.2 ± 4.2	0.2 ± 0.2	−0.0 ± 0.1	8.5/3.5
No Chappuis	0.1 ± 6.0	0.3 ± 0.8	−0.2 ± 4.4	7.0/3.0
No up-looking	13.1 ± 15.0	0.3 ± 0.3	12.8 ± 17.7	4.7/3.3
No up-looking 75°	−1.8 ± 6.1	0.0 ± 0.3	−1.8 ± 4.8	7.3/3.4
SZA 0°	−0.7 ± 5.6	0.3 ± 0.2	−1.0 ± 4.1	7.7/4.0
SZA 75°	0.9 ± 5.8	0.3 ± 0.4	0.3 ± 2.2	7.0/3.0
VZA 75°[b]	0.7 ± 5.8	0.4 ± 0.7	0.6 ± 4.3	7.5/3.6
Surface albedo 0.6	−0.0 ± 5.8	0.0 ± 0.1	−0.1 ± 4.2	7.7/3.8
High tropospheric O_3	0.0 ± 5.9	0.0 ± 0.3	0.0 ± 4.3	7.6/3.7
Low tropospheric O_3	1.1 ± 5.8	0.4 ± 0.3	0.7 ± 4.3	7.5/3.6
Aircraft at 10.2 km	−2.0 ± 9.5	0.3 ± 0.3	−2.5 ± 8.0	7.0/2.8
Aircraft at 5.5 km	2.4 ± 12.6	0.3 ± 0.2	2.1 ± 11.2	6.4/1.8

Note: Columns 2–4 list biases and retrieval errors for the total O_3 column and for O_3 below and above the aircraft, respectively. The two numbers in the DFS column are for the atmosphere and below the aircraft, respectively.
[a]The description lists the difference compared with the base case.
[b]Down-looking direction.

the zenith-sky reference is used or on exclusion of the Chappuis bands. The latter reduces only the information content from the lower troposphere and does not affect retrieval above the aircraft. In practice it might be better not to use the Chappuis bands because it is difficult to account for the pressure- and temperature-dependent absorption of highly variable water vapor. In addition there is a lack of high-quality measured O_3 absorption cross sections in the Chappuis bands. Available cross sections in the visible tend to have slight inconsistencies with O_3 absorption cross sections in the Huggins bands.[43]

For the case in which an external solar spectrum is used as a reference, the biases and errors in the total column and the columns above and below the aircraft are reduced, and the DFS is increased by 1.1 for above the aircraft. If an accurate solar spectrum were available from spaceborne measurements, upper-stratospheric O_3 abundance could also be accurately measured. The disadvantage of using an external solar spectrum is that its use could induce errors from relative wavelength and radiometric calibration. The absence of up-looking measurements has little effect on retrieval below the aircraft, but there are great biases in the total O_3 and O_3 above the aircraft, with a DFS from above of only 1.4, as expected based on Fig. 1. The exclusion of up-looking 75° from the base case has little effect on the retrieval since the DFS decreases by only ~0.1. But when the flight altitude decreases or the SZA increases, the extinction along the path increases because of increasing Rayleigh scattering or the increasing path itself, the sensitivity to O_3 at higher altitudes decreases more for measurements at a VZA of 85° than at 75°, and combining both angles becomes more important. For example, for a SZA of 75° or a flight altitude of 5.5 km (other conditions remain unchanged) the inclusion of up-looking of 75° increases the DFS by ~0.4. Table 2 also shows that the retrieval slightly improves for a larger surface albedo, smaller SZA, and larger down-looking VZA. With a decreasing flight altitude the altitude range where O_3 can be accurately measured is reduced accordingly, and the accuracy in total O_3 is reduced even though the DFS that can be measured above the aircraft increases.

5. Conclusions

A new technique has been demonstrated for retrieving tropospheric O_3 profiles from airborne UV/visible spectrometer measurements. This technique is particularly sensitive to tropospheric O_3 below and ~8 km above the aircraft with a vertical resolution of ~2–6 km and is sensitive to lower and middle stratospheric O_3 with a vertical resolution of 8–15 km. The profile retrieval uses any single down-looking angle and two up-looking angles at 85° and 75° to provide O_3 information below and above the aircraft, respectively. The profiling takes advantage of the wavelength-dependent photon path lengths from below and above the aircraft as well as temperature-dependent O_3 absorption in the Huggins bands and the weakly O_3-absorbing Chappuis bands. Measure-

ments are normalized to direct irradiances or zenith-sky radiances so that this approach does not require the use of an independent solar reference spectrum. With the scanning capability of the proposed instrument this technique can measure tropospheric O_3 at a spatial resolution of 2 km $\times$ 2 km or even higher and therefore is well suited for monitoring regional tropospheric O_3 and validation of satellite measurements of tropospheric O_3.

References

1. G. P. Brasseur, J. T. Kiehl, J.-F. Muller, T. Schneider, C. Granier, X. X. Tie, and D. Hauglustaine, "Past and future changes in global tropospheric ozone: impact on radiative forcing," Geophys. Res. Lett. **25**, 3807–3810 (1998).

2. P. J. Crutzen, "Tropospheric ozone: an overview," in *Tropospheric Ozone*, Regional, and Global Scale Interaction, NATO ASI Series, D. Reidel, ed. (Springer-Verlag, New York, 1988), pp. 3–32.

3. J. Fishman, C. E. Watson, J. C. Larsen, and J. A. Logan, "Distribution of tropospheric ozone determined from satellite data," J. Geophys. Res. **95**, 3599–3617 (1990).

4. J. H. Kim, R. D. Hudson, and A. M. Thompson, "A new method of deriving time-averaged tropospheric column ozone over the tropics using Total Ozone Mapping Spectrometer (TOMS) radiances: intercomparison and analysis using TRACE-A data," J. Geophys. Res. **101**, 24317–24330 (1996).

5. J. Fishman and V. G. Brackett, "The climatological distribution of tropospheric ozone derived from satellite measurements using Version 7 Total Ozone Mapping Spectrometer and Stratospheric Aerosol and Gas Experiment data sets," J. Geophys. Res. **102**, 19275–19278 (1997).

6. R. D. Hudson and A. M. Thompson, "Tropical tropospheric ozone from a Total Ozone Mapping Spectrometer by a modified residual method," J. Geophys. Res. **103**, 22129–22145 (1998).

7. J. R. Ziemke, S. Chandra, and P. K. Bhartia, "Two new methods for deriving tropospheric column ozone from TOMS measurements: assimilated UARS MLS/HALOE and convective-cloud differential techniques," J. Geophys. Res. **103**, 22115–22127 (1998).

8. J. Fishman and A. E. Balok, "Calculation of daily tropospheric ozone residuals using TOMS and empirically improved SBUV measurements: application to an ozone pollution episode over the eastern United States," J. Geophys. Res. **104**, 30319–30340 (1999).

9. M. J. Newchurch, D. Sun, J. H. Kim, and X. Liu, "Tropical tropospheric ozone derived using Clear-Cloudy Pairs (CCP) of TOMS measurements," Atmos. Chem. Phys. **3,** 683–695 (2003).

10. P. J. M. Valks, R. B. A. Koelemeijer, M. van Weele, P. van Velthoven, J. P. F. Fortuin, and H. Kelder, "Variability in tropical tropospheric ozone: analysis with Global Ozone Monitoring Experiment observations and a global model," J. Geophys. Res. **108**, doi:10.1029/2002.JD002894 (2003).

11. S. Chandra, J. R. Ziemke, and R. V. Martin, "Tropospheric ozone at tropical and middle latitudes derived from TOMS/MLS residual: comparison with a global model," J. Geophys. Res. **108**, 4291, doi:4210.1029/2002JD002912 (2003).

12. Y. Jiang and Y. L. Yung, "Concentrations of tropospheric ozone

from 1979 to 1992 over tropical Pacific South America from TOMS data," Science **272,** 714–716 (1996).

13. J. H. Kim and M. J. Newchurch, "Climatology and trends of tropospheric ozone over the eastern Pacific Ocean: the influences of biomass burning and tropospheric dynamics," Geophys. Res. Lett. **23,** 3723–3726 (1996).

14. M. J. Newchurch, X. Liu, and J. H. Kim, "Lower tropospheric ozone (LTO) derived from TOMS near mountainous regions," J. Geophys. Res. **106,** 20403–20412 (2001).

15. J. H. Kim and M. J. Newchurch, "Biomass-burning influence on tropospheric ozone over New Guinea and South America," J. Geophys. Res. **103,** 1455–1461 (1998).

16. J. R. Ziemke, S. Chandra, and P. K. Bhartia, "Cloud slicing: a new technique to derive upper tropospheric ozone from satellite measurements," J. Geophys. Res. **106,** 9853–9867 (2001).

17. M. Newchurch, D. Sun, X. Liu, L. Emmons, L. Horowitz, J. H. Kim, D. Kinnison, G. Brasseur, D. Jacob, J. Logan, R. V. Martin, K. Han, and S. Na, "Critical assessment of TOMS-derived tropospheric ozone: comparisons with other measurements and model evaluation of controlling processes," Eos. Trans. Am. Geophys. Union **82,** Spring Meeting Supplement, Abstract A52A-09 (2001).

18. R. Munro, R. Siddans, W. J. Reburn, and B. Kerridge, "Direct measurement of tropospheric ozone from space," Nature (London) **392,** 168–171 (1998).

19. R. Hoogen, V. V. Rozanov, and J. P. Burrows, "Ozone profiles from GOME satellite data: algorithm description and first validation," J. Geophys. Res. **104,** 8263–8280 (1999).

20. O. P. Hasekamp and J. Landgraf, "Ozone profile retrieval from backscattered ultraviolet radiances: the inverse problem solved by regularization," J. Geophys. Res. **106,** 8077–8088 (2001).

21. R. J. van der A, R. F. van Oss, A. J. M. Piters, J. P. F. Fortuin, Y. J. Meijer, and H. M. Kelder, "Ozone profile retrieval from recalibrated GOME data," J. Geophys. Res. **107,** doi:10.1029/2001JD000696 (2002).

22. K. Chance, X. Liu, R. J. D. Spurr, T. P. Kurosu, C. E. Sioris, R. V. Martin, M. J. Newchurch, and P. K. Bhartia, "Ozone profile retrieval from the Global Ozone Monitoring Instrument," in *Proceeding of the XX Quadrennial Ozone Symposium*, C. S. Zerefos, ed. (International Ozone Commission, Athens, Greece, 2004), pp. 483–484.

23. A. Wahner, J. Callies, H.-P. Dorn, U. Platt, and C. Schiller, "Near UV atmospheric absorption measurements of column abundances during Airborne Arctic Stratospheric Expedition, January–February 1989: 3. BrO observations," Geophys. Res. Lett. **17,** 517–520 (1990).

24. A. Wahner, J. Callies, H.-P. Dorn, U. Platt, and C. Schiller, "Near-UV atmospheric absorption measurements of column abundances during Airborne Arctic Stratospheric Expedition, January–February 1989: 1. Technique and NO_2 observations," Geophys. Res. Lett. **17,** 497–500 (1990).

25. C. Schiller, A. Wahner, U. Platt, H.-P. Dorn, J. Callies, and D. H. Ehhalt, "Near-UV atmospheric absorption measurements of column abundances during Airborne Arctic Stratospheric Expedition, January–February 1989: 2. OClO observations," Geophys. Res. Lett. **17,** 501–504 (1990).

26. R. Brandtjen, T. Klüpfel, D. Perner, and B. M. Knudsen, "Airborne measurements during the European Arctic Stratospheric Ozone Experiment: observation of OClO," Geophys. Res. Lett. **21,** 1363–1366 (1994).

27. K. Pfeilsticker and U. Platt, "Airborne measurements during the Arctic stratospheric experiment: observation of O_3 and NO_2," Geophys. Res. Lett. **21,** 1375–1378 (1994).

28. N. Glatthor, C. E. Blom, T. von Clarmann, H. Fischer, T. Gulde, C. Piesch, F. Erle, K. Pfeilsticker, M. P. Chipperfield, A. M. Lee, and J. A. Pyle, "Airborne remote sensing of NO_2 in the Arctic winter of 1994–1995 and comparison with a three-dimensional chemical transport model," J. Geophys. Res. **103,** 13315–13326 (1998).

29. Y. Jiang, Y. L. Yung, and S. P. Sander, "Detection of tropospheric ozone by remote sensing from the ground," J. Quant. Spectrosc. Radiat. Transfer **57,** 811–818 (1997).

30. A. Petritoli, F. Ravegnani, G. Giovanelli, D. Bortoli, U. Bonafe, I. Kostadinov, and A. Oulanovsky, "Off-axis measurements of atmospheric trace gases by use of an airborne ultraviolet–visible spectrometer," Appl. Opt. **41,** 5593–5599 (2002).

31. T. Wagner, M. Bruns, J. P. Burrows, S. Fietkau, F. Finocchi, K.-P. Heue, G. Honninger, U. Platt, I. Pundt, A. Richter, R. Rollenbeck, C. v. Friedeburg, F. Wittrock, and P. Xie, "The AMAXDOAS instrument and its application for SCIAMACHY validation," presented at the 15th European Space Agency Symposium on European Rocket and Balloon Programmes and Related Research, Biarritz, France, 28–31 May 2001.

32. M. Bruns, S. A. Buehler, J. P. Burrows, K.-P. Heue, U. Platt, I. Pundt, A. Richter, A. Rozanov, T. Wagner, and P. Wang, "Retrieval of profile information from airborne multiaxis UV/visible skylight absorption measurements," Appl. Opt. **43,** 4415–4426 (2004).

33. C. D. Rodgers, *Inverse Methods for Atmospheric Sounding: Theory and Practice* (World Scientific, Singapore, 2000).

34. L. Harrison, J. Michalsky, and J. Berndt, "Automated multi-filter rotation shadow-band radiometer: an instrument for optical depth and radiation measurements," Appl. Opt. **33,** 5118–5125 (1994).

35. F. X. Kneizys, E. P. Shettle, L. W. Abreu, J. H. Chetwynd, G. P. Anderson, W. O. Gallery, J. E. A. Selby, and S. A. Clough, "Users Guide to LOWTRAN 7," AFGL-TR-88-0177 (Air Force Geophysics Laboratory, Hanscom AFB, Mass., 1988).

36. O. Torres, P. K. Bhartia, J. R. Herman, Z. Ahmad, and J. Gleason, "Derivation of aerosol properties from satellite measurements of backscattered ultraviolet radiation: theoretical basis," J. Geophys. Res. **103,** 17099–17110 (1998).

37. Y. J. Kaufman, D. Tanre, L. A. Remer, E. F. Vermote, A. Chu, and B. N. Holben, "Operational remote sensing of tropospheric aerosol over land from EOS moderate resolution imaging spectroradiometer," J. Geophys. Res. **102,** 17051–17067 (1997).

38. J. R. Acarreta and J. F. de Haan, "Cloud pressure algorithm based on O_2–O_2 absorption," in *OMI Algorithm Theoretical Basis Document*, Vol. III: Clouds, Aerosols, and Surface UV Irradiance, P. Stammes, ed. (http://eospso.gsfc.nasa.gov/eos homepage/for scientists/atbd/docs/OMI/ATBD-OMI-03.pdf.

39. R. V. Martin, K. Chance, D. J. Jacob, T. P. Kurosu, R. J. D. Spurr, E. Bucsela, J. F. Gleason, P. I. Palmer, I. Bey, A. M. Fiore, Q. Li, R. M. Yantosca, and R. B. A. Koelemeijer, "An improved retrieval of tropospheric nitrogen dioxide from GOME," J. Geophys. Res. **107,** doi:10.1029/2001JD001027 (2002).

40. K. V. Chance, J. P. Burrows, D. Perner, and W. Schneider, "Satellite measurements of atmospheric ozone profiles, including tropospheric ozone, from ultraviolet/visible measurements in the nadir geometry: a potential method to retrieve tropospheric ozone," J. Quant. Spectrosc. Radiat. Transfer **57,** 467–476 (1997).

41. R. J. D. Spurr, T. P. Kurosu, and K. V. Chance, "A linearized discrete ordinate radiative transfer model for atmospheric remote-sensing retrieval," J. Quant. Spectrosc. Radiat. Transfer **68,** 689–735 (2001).

42. R. D. McPeters, J. A. Logan, and G. J. Labow, "Ozone climatological profiles for Version 8 TOMS and SBUV retrievals," Eos. Trans. Am. Geophys. Union **84,** Fall Meeting Supplement, Abstract A21D-0998 (2003).

43. J. Orphal, "A critical review of the absorption cross sections of O_3 and NO_2 in the 240–790-nm region," J. Photochem. Photobiol. A **157,** 185–209 (2003).